Strong effective saturation by optical pumping in three-level systems

J. I. Kim, D. Haubrich, B. Klöter, and D. Meschede
Institut für Angewandte Physik, Universität Bonn, Wegelerstraße 8, 53115 Bonn, Germany
(Received 14 April 2009; published 2 December 2009)

We have studied nonlinear absorption from the In $P_{1/2,3/2}$ ground-state doublet in a resistively heated high-temperature cell and a hollow cathode lamp. Using probe and pump lasers at 410 and 451 nm, respectively, absorption spectra with nonlinear properties caused by saturated absorption, coherent dark resonances, and optical pumping are observed. A theoretical description in terms of a density-matrix theory agrees very well with the observed spectra and identifies optical pumping as a dominating process of broadening in the stepwise contribution rather than velocity-changing collisions. Our experiments suggest that the theory used here is widely applicable in saturation spectroscopy on three-level Λ systems.

DOI: 10.1103/PhysRevA.80.063801 PACS number(s): 42.62.Fi, 32.30.Jc, 32.70.Jz, 42.55.Px

I. INTRODUCTION

Saturation spectroscopy is a very widely used method not only to obtain information about the physical properties of, e.g., atomic or molecular vapors [1,2]. It is also used in numerous laboratories to stabilize narrow-band lasers to certain resonance wavelengths. In our laboratory, we apply this method to stabilize lasers to blue and violet resonance wavelengths of the In atom. We study In in our laboratory with respect to its applicability for laser cooling [3,4] and in atomic nanofabrication [5]. In other experiments, we apply the same concept with alkali vapors.

In more than 30 years of saturation spectroscopy, an enormous body of literature has been accumulated on this topic, both from the theoretical point and the experimental point of view and mostly demonstrated with alkali vapors. Saturation spectra are typically measured in absorption from vapor cells and consist of a group of narrow lines reflecting the fine structure of the vapor atoms together with a Doppler broadened background. Therefore, the observation of strong lines with a vapor of In atoms with intermediate line width remains unusual and raises the question of their physical origin [6].

It is well known that optical pumping plays an important role in saturation spectroscopy [7–10] and becomes especially significant if three or more levels are involved. Most importantly, optical pumping induces a redistribution of atomic populations between relevant internal levels. In alkali vapors, the most widely used physical system in saturation spectroscopy, the Λ-type multilevel systems, are based on two or more hyperfine ground states with energy separation negligible with respect to thermal energies and hence initially evenly populated. Interaction with two resonant laser beams drives the two-photon Λ transition and causes some redistributions by optical pumping, but the distortion of the well-known spectral line shapes, a Doppler spectrum with narrow saturation dips, remains small and is usually ignored [11,12].

Elements of the third group of the periodic table (Al, In, Ga) have a similar structure, but the spacing of the two fine-structure ground states widely exceeds thermal energies. In striking contrast to alkali atom vapors, the population is initially concentrated in only one of the two levels. In this case, optical pumping strongly affects the relative thermal populations. As a consequence, the gross line shapes obtained by laser spectroscopy with typical vapor cells are now even dominated by optical pumping. They have neither Doppler nor Doppler-free character.

In this paper, we explicit an interpretation of spectroscopic line shapes obtained in saturation spectroscopy with In vapor cells in terms of a perturbative density-matrix treatment given by Berman *et al.* [13] 30 years ago. The model is perturbative only in the probe field and includes stepwise and coherent two-photon processes as well as velocity changing collisions (VCCs). We show that it explains the unusual observed line shapes. It leaves no room for our earlier phenomenological interpretation of a broad but sub-Doppler contribution to the line shape in terms of VCCs which plays a minor role in the line shape in low vapor pressure cells [6].

The work by Berman *et al.* was in 1979 directed toward the role of VCCs. Also, at that time, numerical evaluation of the theory and comparison to experimental data were much more involved than with today's convenient computer algebra. With this paper, we show that the theory presented in [13] gives very good agreement with experimental data and furthermore provides a detailed understanding of relevant physical processes.

II. EXPERIMENTS AND RESULTS

We have recorded and analyzed saturation spectra involving two laser frequencies with In vapor cells. We have used two different Λ systems. In one case, two closely spaced hyperfine levels of the In atom were coupled to an excited state and in the other case, two widely spaced fine-structure levels were used.

Relevant atomic levels of the In atom are shown in Fig. 1. The $5P_{1/2}$, $5P_{3/2}$ ground-state doublet is connected to the first-excited $6S_{1/2}$ state in terms of a three-level, Λ-type configuration. Violet laser light at $\lambda_{\mathrm{vio}}=\lambda_{6S_{1/2}\rightarrow 5P_{1/2}}=410$ nm is available from diode lasers and blue light at $\lambda_{\mathrm{blue}}=\lambda_{6S_{1/2}\rightarrow 5P_{3/2}}=451$ nm from a frequency doubled Ti:sapphire laser. The branching ratio of the $6S_{1/2}\rightarrow 5P_{1/2}$:$6S_{1/2}\rightarrow 5P_{3/2}$ is about 2:3. The decay rates for the relevant channels are given in Table I. The saturation intensities of each transition are calculated from a rate equation model.

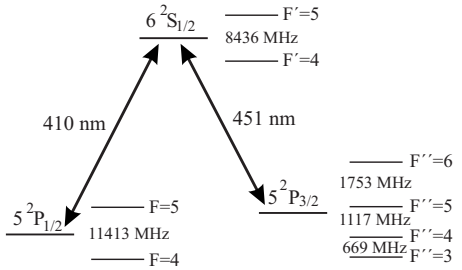

FIG. 1. Energy level scheme of ^{115}In. The lasers in the experiment address $5P_{1/2}$, $F=4$, 5 to $6S_{1/2}$, $F'=5$ transitions for ASC experiment and $5P_{1/2}$, $F''=5$, 6 to $6S_{1/2}$, $F'=5$ transitions for HCL experiment.

At room temperature, the In vapor pressure is very low and only a small fraction $[N(P_{3/2})=0.005\%]$ of the In atoms are in the $5P_{3/2}$ state. Thus, special cells generating high-density In vapors are required to probe especially the $5P_{3/2}\rightarrow 6S_{1/2}$ transition at 451 nm.

We have used two vapor cells: (1) a high-temperature all-sapphire cell (ASC) [6] which was resistively heated up to 600 °C. However, even at the maximum temperature, the population of the elevated $5P_{3/2}$ level and hence the $5P_{3/2}\rightarrow 6S_{1/2}$ transition strength remained weak. Thus we constructed in addition (2) a hollow cathode lamp (HCL) generating a high-density vapor by sputtering. It is operated near ambient temperatures and shows strong resonant absorption of both fine-structure transitions $5P_{1/2,3/2}\rightarrow 6S_{1/2}$. The HCL furthermore reduces experimental problems caused by the high-temperature oven which impairs experiments by, e.g., generation of air currents.

(1) All sapphire cell. At about 600 °C, the In vapor shows an absorption coefficient of order $\alpha\sim 0.03$ cm^{-1} for the violet $5P_{1/2}(F=4,5)\rightarrow 6S_{1/2}(F'=5)$ transitions at 410 nm with probe beam $F=4\rightarrow F'=5$ and pump beam $F=5\rightarrow F'=5$. An absorption spectrum of the probe beam (0.1 mW) with and without pump beam (1.5 mW) is shown in Fig. 2. The absorption spectrum in the presence of the pump beam can be associated with three different contributions: the Doppler-limited background [full width at half maximum (FWHM) $\sim$1270 MHz], an additional broad Lorentzian-like contribution (FWHM$\sim$311 MHz), and a narrow Lorentzian (FWHM$\sim$4 MHz) substantially below the natural linewidth of 25 MHz at the center of the broader lines.

In Fig. 2(b) we show the difference of the absorption spectrum for the $5P_{1/2}(F=4,5)\rightarrow 6S_{1/2}(F'=5)$ transition

TABLE I. Selected parameters for optical transitions of ^{115}In.

Property	Symbol	Value
Total decay rate of $6S_{1/2}$	$\Gamma/2\pi$	25.1 MHz
Branching rate $6S_{1/2}\rightarrow 5P_{3/2}$	$\Gamma_{451}/2\pi$	16.2 MHz
Branching rate $6S_{1/2}\rightarrow 5P_{1/2}$, $F=5$	$\Gamma_1/2\pi$	3.5 MHz
Branching rate $6S_{1/2}\rightarrow 5P_{1/2}$, $F=4$	$\Gamma_2/2\pi$	5.3 MHz
Saturation intensity in $5P_{1/2}\rightarrow 6S_{1/2}$	$I_{\rm sat}^{410}$	15.9 mW/cm^2
Saturation intensity in $5P_{3/2}\rightarrow 6S_{1/2}$	$I_{\rm sat}^{451}$	11.9 mW/cm^2

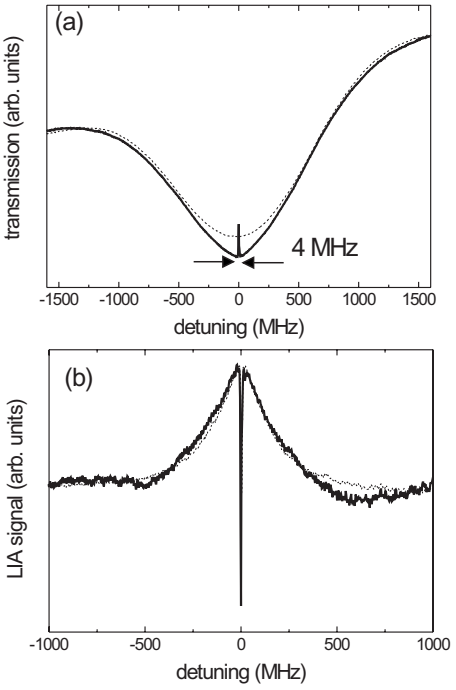

FIG. 2. ASC. (a) Absorption spectra of the probe beam with (solid line) and without (dashed line) the pump beam tuned to the center of the Doppler broadened spectrum. The slanted intensity is due to diode laser power variation. (b) Difference (solid line) of the two spectra from (a) compared to absorption signal demodulated by a lock-in amplifier (dotted line).

without and with pump beam which we call "LIA signal" (laser induced absorption signal) for the sake of brevity. For comparison, we refer to Fig. 3 from [6] where a second Λ system was investigated: The $5P_{1/2}(F=4)\rightarrow 6S_{1/2}(F'=5)$ was used as a pump beam while the $5P_{3/2}(F''=4,5,6)\rightarrow 6S_{1/2}(F'=5)$ transitions were probed (two-color spectroscopy). Here, the LIA signal was obtained by demodulation with a lock-in amplifier. The spectrum shows the same prominent features observed in Fig. 2(b): the broad Lorentzian-like line shape with sub-Doppler width and the narrow dip which is straightforwardly interpreted as a consequence of coherent population trapping leading to electromagnetically induced transparency (EIT).

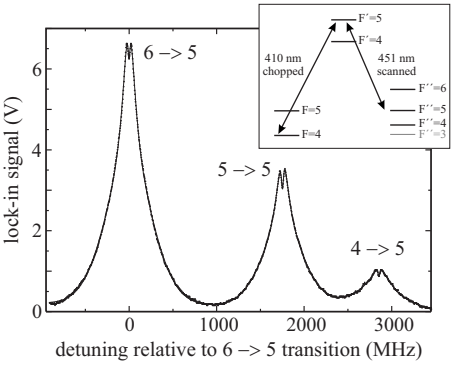

FIG. 3. ASC. Demodulated absorption spectra of the probe beam in the presence of the pump beam as a function of the detuning of the probe-laser frequency in the two-color spectroscopy [6].

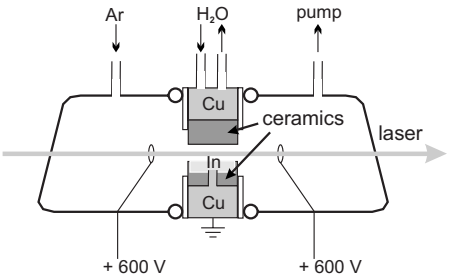

FIG. 4. Schematic drawing of the hollow cathode lamp. The cathode is made of pure indium which is inserted into a crucible made of nonconducting ceramic (dark gray). The indium pool is grounded by a copper inlet (light gray) at the bottom of the crucible. The crucible has a length of 30 mm and a clearance of 5 mm above the indium pool.

For the present paper, we reanalyze the LIA line shapes in Sec. III, with special emphasis on the broad but sub-Doppler contribution (LIA signal) prominent in Figs. 2 and 3. We apply a first-principles theoretical model to the Λ system involving the hyperfine levels $F=4,5$ of the $5P_{1/2}$ state but equally applicable to the system involving the two fine-structure states $5P_{1/2,3/2}$. The time scale is set by the atomic lifetime which is short compared to the time spent within the laser beams (average transit times 2.8 μs vs. 6.6 ns). Thus a steady-state model is sufficient.

(2) Hollow cathode lamp. An alternative source of atomic vapor is a hollow cathode lamp (HCL) providing robust and compact atomic references [14,15]. Our construction is specially designed for materials with low melting points (In: 156 °C) that cannot directly be used to make massive electrodes. It closely resembles the concept presented in [16] and outlined in Fig. 4. We find that it produces excellent absorption column densities without the need of high operating temperatures. It generates a vapor density equivalent to a temperature in excess of 1000 °C; the population in the upper fine-structure ground state is $N(P_{3/2})=18\%$. Furthermore, it eliminates the need for buffer gas that impairs the application of Doppler-free methods of laser spectroscopy for laser stabilization [17].

The cathode is made of pure indium which is inserted into a crucible made of nonconducting ceramic. At the bottom of the crucible, a copper inlet ensures electric conductivity between the indium pool and the outer grounded copper casing. When the indium melts during normal discharge operation, it remains confined to this reservoir. The crucible has a length of $L=30$ mm and free space of 5 mm above the indium pool. The whole cathode block is water-cooled to 17 °C. The anode is made of two stainless-steel rings which are mounted 5 mm to the sides of the cathode holder. The assembly of two Pyrex tubes and a central cathode is clamped together and sealed with o-rings. The cell pressure is sustained by a roughing pump at a level of 500 Pa while venting the cell with argon gas which ensures a stable discharge. The discharge current is supplied by a 2 kV voltage power supply with a maximum current of 100 mA dc. The minimum current at which we can observe a stable discharge is about 20 mA. The electrical resistance of the discharge is approximately 6 kΩ.

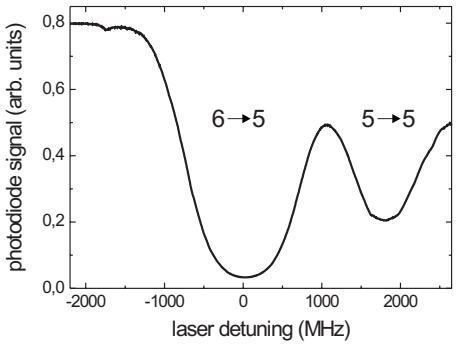

FIG. 5. HCL. Doppler-broadened transmission spectrum of the 451 nm probe laser for the $5P_{3/2}$, $F''=6$, $5\rightarrow 6S_{1/2}$, $F'=5$ transitions. Discharge current 40 mA.

A single laser beam ($\lambda=451$ nm) with intensity $0.08I_{\mathrm{sat}}^{451}$ passes just above the In reservoir through the cell. The transmitted intensity is measured with a photodiode behind the cell as a function of laser frequency for different discharge currents. The laser frequency is scanned across the $F''=6\rightarrow F'=5$ transition at 451 nm. Figure 5 shows the strong, Doppler-broadened absorption lines at a discharge current of 40 mA. The dips correspond to the $F''=6\rightarrow F'=5$ transition for the larger one and the $F''=5\rightarrow F'=5$ transition for the smaller one. The minima of the two peaks serve as a frequency calibration for the lower axis. The absorption for the larger dip $(6\rightarrow 5)$ is $(95\pm 3)\%$ and the FWHM is $\Delta\nu=(1620\pm 20)$ MHz. The flattened line shape in the Fig. 5 is attributed to the saturation.

In the HCL, we have achieved a high effective temperature and a convenient column density. By measuring the FWHMs of Doppler-broadened transmission spectra and absorptions, a temperature is measured to be 1236 °C yielding a column density of 3.8×10^{17} m^{-3} at 55 mA discharge current.

For Doppler-free polarization spectroscopy, a circularly polarized laser beam (pump beam) is shone in counterpropagating to the linear polarized first beam (probe beam) as shown in Fig. 6. It is amplitude modulated with a chopper wheel rotating at a frequency of 1.4 kHz. The probe beam is split behind the HCL with a polarizing beam splitter cube (PBSC) oriented 45° with respect to the polarization axis of

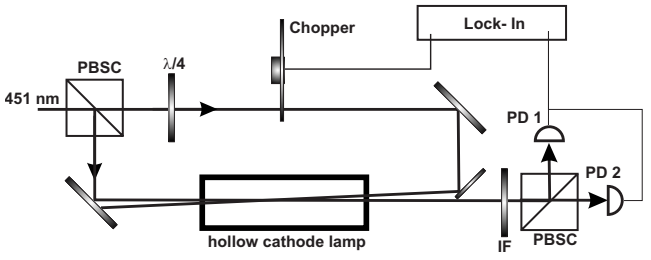

FIG. 6. Setup for spectroscopy with the HCL. The incoming laser beam is split in half by a PBSC and guided through the HCL. The pump beam is circular polarized and can be amplitude modulated with a chopper wheel. The polarization of the probe beam behind the HCL is analyzed with photodiodes PD1 and PD2 and demodulated with a lock-in amplifier. An interference filter (IF) blocks light caused by the discharge.

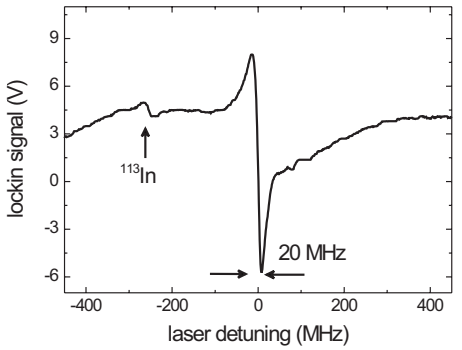

FIG. 7. HCL. Doppler-free spectrum of the $5P_{3/2}$, $F''=6\rightarrow 6S_{1/2}$, $F'=5$ resonance line, demodulated by polarization spectroscopy. The small dispersive signal corresponds to the ^{113}In isotope.

the beam. The two output beams are detected with photodiodes and subtracted. An interference filter in front of the PBSC blocks all light generated by the discharge. The difference signal of the photodiodes is analyzed with a lock-in amplifier.

Figure 7 shows the resulting dispersive signal which is typical for polarization spectroscopy with an additional Doppler base of (140 ± 10) MHz. The width of the dispersive signal is (20 ± 1) MHz. The smaller signal which is about 275 MHz below the large resonance belongs to the ^{113}In isotope which has a natural abundance of 4.3%. The dispersive signal was used as an error signal for a feedback circuit to reduce slow drifts of the Ti:sapphire laser. Since the discharge is robust, laser stabilization is ensured for hours.

III. LINE SHAPE ANALYSIS

We consider a model treating the indium atoms as a three-level, Λ-type system coupled by the pump and probe beam. The pump (Rabi frequency Ω_1) and probe (Rabi frequency Ω_2) are coupled to the $5\rightarrow 5$ and $4\rightarrow 5$ transitions, respectively. Further hyperfine levels do not influence the absorption of the probe beam. However, they are responsible for additional loss channels in the excited state. These losses lead to significant depopulation by optical pumping resulting in a large effective saturation parameter and playing a crucial role for understanding the broad sub-Doppler contribution.

In Fig. 8(a), we show the simplified energy-level scheme. The excited state decays to the coupled ground state with rates Γ_i $(i=1,2)$ and to other uncoupled ground states with rates $\Gamma-\Gamma_1-\Gamma_2$, where Γ is the total decay rate of the excited state. Atoms from uncoupled states eventually leave the laser beam and in turn "fresh atoms" with statistical population of ground-state levels replenish the reservoir of atoms. In a simplified model, we account for this process through effective ground-state decay and pump rates $\gamma=\gamma_1=\gamma_3$.

Such three-level systems have been intensely studied for decades. For instance, Berman has described a perturbative density-matrix theory including velocity changing collisions in Ref. [13]. More detailed equations are reproduced in Appendix A. We find that for our experimental conditions, the term accounting for velocity changing collisions gives only

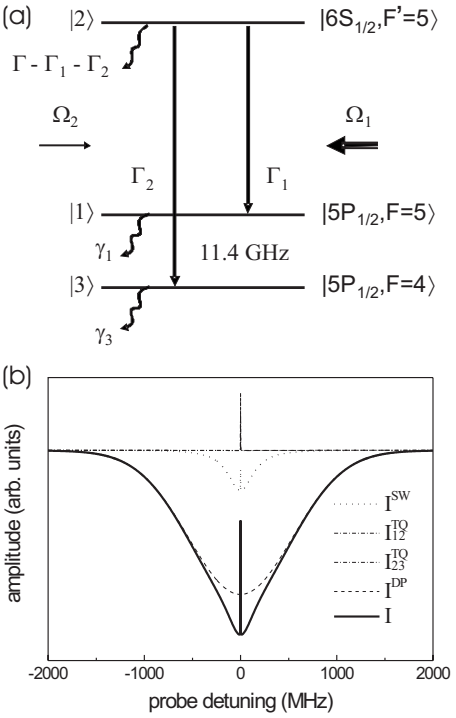

FIG. 8. (a) Simplified energy-level scheme of indium with pump and probe transitions; γ_i, effective decay rate of the ground states; Γ,Γ_i, total and partial decay rate of the excited state; Ω_i, Rabi frequencies. (b) The calculated probe beam absorption spectrum with (solid line) and without pump beam (dashed line). Also, the contributions of the coherent two-photon processes (dashed-dotted lines) and step wise contribution (dotted line) are shown.

negligible contributions and can hence be omitted. Thus we have to correct our earlier interpretation [6] where the origin of the intermediate linewidth contribution was associated with this cause.

The final form of the expressions of the absorption of the probe applying to our experiment is hence

$$I(\Delta_1,\Delta_2)=I_{12}^{\mathrm{TQ}}+I_{23}^{\mathrm{TQ}}+I^{\mathrm{SW}}+I^{\mathrm{DP}}, \tag{1}$$

where Δ_1 and Δ_2 are the pump and probe detunings, respectively, and

$$I_{12}^{\mathrm{TQ}}=\frac{N_{21}(\Omega_1\Omega_2)^2}{8\gamma(k_1u)[(k_2-k_1)u](k_2u)}\mathrm{Im}\sum_{i=1}^{4}A_iZ(r_i),$$

$$I_{23}^{\mathrm{TQ}}=N_{32}\frac{\Omega_2^2}{2\gamma(k_2u)}\mathrm{Im}\sum_{i=1}^{2}[B_iZ(r_i)-Z(r_7)],.$$

$$I^{\mathrm{SW}}=\left(1-\frac{\Gamma_2}{\gamma}\right)\frac{N_{21}(\Omega_1\Omega_2)^2}{8\gamma(k_1u)^2(k_2u)}\mathrm{Im}\sum_{i=1}^{4}D_iZ(r_i),$$

$$I^{\mathrm{DP}}=N_{32}\frac{\Omega_2^2}{2\gamma(k_2u)}\mathrm{Im}\,Z(r_7), \tag{2}$$

where k_i is the wave number, $Z(r_i)$ is the plasma dispersion function, and u is the most probable velocity of atoms. All

TABLE II. Parameters of ^{115}In for a theoretical model.

Property	Symbol	Value
$N(F'=5)-N(F=5)$ at 600 °C	N_{21}	−0.5
$N(F=4)-N(F'=5)$ at 600 °C	N_{32}	0.4
Rabi frequency of pump	Ω_1	0.5Γ
Rabi frequency of probe	Ω_2	0.15Γ
Decay rate between ground states	γ_{13}	0.01Γ
Decay rate of ground states	γ	$1.6(0.1)\times 10^{-3}\Gamma$

constants used in Eq. (2) (A_i, B_i, D_i, r_i) are identical to those used in Ref. [13]. For illustration, the four individual calculated contributions are shown in Fig. 8(b) along with the total absorption line shapes with and without pump beam.

In Eq. (1), the first and second terms are the two quanta (TQ) contributions which are caused by coherent two-photon coupling of the long-lived ground states (matrix element ρ_{13}) only. The stepwise (SW) contribution involves population of the excited intermediate state (ρ_{22}), i.e., sequential absorption and emission of a photon, also into uncoupled states [18]. The fourth term represents the Doppler-limited absorption of the probe beam in the absence of the pump beam. The experimental parameters used in the calculations are summarized in Table II. The line shapes of the experimental and theoretical spectra are in good agreement.

While the interpretation of the Doppler line as well as the coherent dark resonance (TQ) is straightforward, the SW term remains somewhat puzzling. It is of approximately Lorentzian line shape and has a width in between typical narrow high-resolution features and the Doppler line width. Theoretically, the FWHM of the SW term is determined by a parameter [13]

$$\mathrm{FWHM}_{\mathrm{SW}} = \Gamma\sqrt{1 + s_{\mathrm{eff}}^{\mathrm{DM}}}, \tag{3}$$

where the defined effective saturation parameter $s_{\mathrm{eff}}^{\mathrm{DM}}$ of the three-level, Λ-type system is defined by

$$s_{\mathrm{eff}}^{\mathrm{DM}} = \frac{\Omega_1^2}{\Gamma}\left[\frac{1}{\Gamma} + \frac{1}{\gamma}\left(1 - \frac{\Gamma_1}{\Gamma}\right)\right]. \tag{4}$$

For a very weak pump field ($s_{\mathrm{eff}}^{\mathrm{DM}} \ll 1$), the saturation parameter can be neglected so that $\mathrm{FWHM}_{\mathrm{SW}} \sim \Gamma$.

The effective pump and decay rate of the ground state γ in Eq. (4) is not known beforehand but can be deduced by measuring the FWHM of the SW component as shown in Fig. 2(b) and as a function of the pump intensity. We extract the FWHM of SW term by fitting two Lorentzian functions (one for the SW, another one for the TQ term). The data are shown in Fig. 9 as a function of the pump beam intensity. By fitting the data with Eq. (4), the value for γ is found to be $1.6(0.1)\times 10^{-3}\Gamma$.

The effective decay rate for the ground states is a rough measure for the rate of atoms entering and leaving the laser beam. Considering the average thermal velocity of In atoms at 600 °C and the beam diameter of the pump beam, this rate is estimated to be $2\times 10^{-3}\Gamma$ which compares well to the value inferred from our measurements. The $s_{\mathrm{eff}}^{\mathrm{DM}}$ based on the measured γ is calculated to be 137 at the pump Rabi frequency $\Omega_1 = 0.5\Gamma$. The solid line in Fig. 9 shows the fitted FWHM of the SW term due to the surprisingly large values for $s_{\mathrm{eff}}^{\mathrm{DM}}$. The very large saturation parameter can be interpreted as a consequence of strong optical pumping in such a three-level, Λ-type system. Typically the pump intensity is much stronger than that of the probe and the ground state of the probe transition experiences almost no decay. Thus, for resonant excitation, atoms are rapidly (in comparison to the transit time of the atoms through the laser beam) pumped to uncoupled states. Even relatively far off-resonance optical pumping remains efficient since small excitation probabilities are compensated by long dwell times within the laser beam ($\tau_{\mathrm{transit}} = 400/\Gamma$).

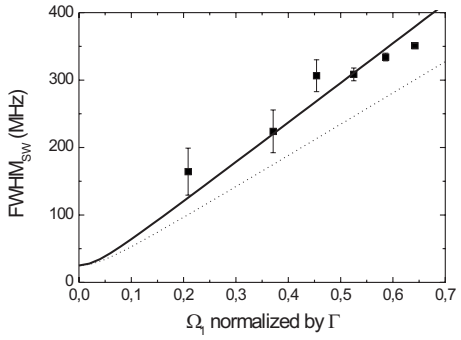

FIG. 9. The FWHM of SW as a function of the Rabi frequency of the pump beam. Data are fitted (solid line) by Eq. (4) yielding $\gamma = 1.6(0.1)\times 10^{-3}\Gamma$. The dotted line is the FWHM deduced by $s_{\mathrm{eff}}^{\mathrm{RE}}$ in a rate equation model for the same γ.

In order to gain more physical insight, we have studied in addition to the full density-matrix treatment a rate equation model which neglects all coherences and compared the effective saturation parameters deduced by the density matrix and rate equation models as outlined in Appendix B. The dotted line in Fig. 9 shows the FWHM of SW term based on the $s_{\mathrm{eff}}^{\mathrm{RE}}$ in a rate equation model.

In addition, we have checked the dependence of $\mathrm{FWHM}_{\mathrm{SW}}$ on the transit time by comparing the spectra for two different beam diameters d (1 and 3 mm) at fixed pump Rabi frequency ($\sim 0.2\Gamma$). For the FWHMs of the LIA signals, we find 164 ± 35 MHz for the small beam and 271 ± 12 MHz for the large beam. In the limit $\gamma \ll \Gamma_i, \Omega_i$, the theoretical ratio should be approximately $\mathrm{FWHM}^{(1\ \mathrm{mm})}/\mathrm{FWHM}^{(3\ \mathrm{mm})} \sim \sqrt{\gamma^{(3\ \mathrm{mm})}/\gamma^{(1\ \mathrm{mm})}} = \sqrt{1\ \mathrm{mm}/3\ \mathrm{mm}} = 0.58$, which compares very well to ratio $164/271 \sim 0.6$.

IV. CONCLUSION

We observed and analyzed open Λ-type two-color transitions with In vapor cells. A perturbative, slightly extended three-level model [13] convincingly and exhaustively explains all aspects of the observed spectra and under different conditions. Especially, we have shown that optical pumping dominates the line shapes observed for saturation spectroscopy in a Λ system with strong initial population imbalance. Our analysis shows that the role of optical pumping can be

quantitatively estimated by introducing an effective saturation parameter based on atomic and experimentally available parameters.

Although numerically a bit involved, this model provides an excellent and fairly general basis for understanding line shapes involving three coupled levels in gas cells. The model simultaneously explains spectroscopic data obtained from Λ-type atomic systems with small and large energy separation of the ground-state doublet. This situation has widespread applicability including vapors of alkali, earth-alkaline, and elements of the third group of the periodic table.

ACKNOWLEDGMENTS

We wish to thank K. A. H. van Leeuwen and his coworkers for building the hollow cathode cell and H. Metcalf and P. Berman for a critical reading of the paper. J.K. is grateful to L. Kong and J. Choi for helpful discussions. J. Mende is thanked for help in setting up the hollow cathode lamp.

APPENDIX A: DENSITY MATRIX EQUATIONS FOR THREE-LEVEL, Λ-TYPE SYSTEM WITH ADDITIONAL LOSS CHANNELS IN INDIUM

In this appendix, the detailed density-matrix equations for a three-level, Λ-type system are described. The steady-state expression of density-matrix equations for the simplified three-level, Λ-type system in Fig. 8 neglecting velocity changing collisions can be written as [13]

$$\gamma\rho_{11}(\vec{v}) = \lambda_1(\vec{v}) + i\frac{\Omega_1}{2}[\rho_{21}(\vec{v}) - \rho_{12}(\vec{v})] + \Gamma_1\rho_{22}(\vec{v}),$$

$$\Gamma\rho_{22}(\vec{v}) = \lambda_2(\vec{v}) - i\frac{\Omega_1}{2}[\rho_{21}(\vec{v}) - \rho_{12}(\vec{v})] - i\frac{\Omega_2}{2}[\rho_{23}(\vec{v}) - \rho_{32}(\vec{v})],$$

$$\gamma\rho_{33}(\vec{v}) = \lambda_3(\vec{v}) + i\frac{\Omega_2}{2}[\rho_{23}(\vec{v}) - \rho_{32}(\vec{v})] + \Gamma_2\rho_{22}(\vec{v}), \tag{A1}$$

$$\mu_{12}(\vec{v})\rho_{12}(\vec{v}) = i\frac{\Omega_1}{2}[\rho_{22}(\vec{v}) - \rho_{11}(\vec{v})] - i\frac{\Omega_2}{2}\rho_{13}(\vec{v}),$$

$$\mu_{23}(\vec{v})\rho_{23}(\vec{v}) = i\frac{\Omega_2}{2}[\rho_{33}(\vec{v}) - \rho_{22}(\vec{v})] + i\frac{\Omega_1}{2}\rho_{13}(\vec{v}),$$

$$\mu_{13}(\vec{v})\rho_{13}(\vec{v}) = i\frac{\Omega_1}{2}\rho_{23}(\vec{v}) - i\frac{\Omega_2}{2}\rho_{12}(\vec{v}), \tag{A2}$$

where $\lambda_i(\vec{v})$ is the incoherent pumping rate related to the population and

$$\mu_{12}(\vec{v}) = \Gamma/2 - i(\Delta_1 - k_1 v_z),$$

$$\mu_{23}(\vec{v}) = \Gamma/2 + i(\Delta_2 - k_2 v_z),$$

$$\mu_{13}(\vec{v}) = \gamma_{13} + i[(\Delta_2 - \Delta_1) - (k_2 - k_1)v_z], \tag{A3}$$

where Δ_i is the detuning and k_i is the wave number.

The value which is equivalent to the absorption is given by [13]

$$I(\Delta_1,\Delta_2) = \mathrm{Im}\int d\vec{v}\left(\rho_{33}(\vec{v}) - \frac{\lambda_3(\vec{v})}{\gamma}\right) = \frac{\Omega_2}{\gamma}\mathrm{Im}\int d\vec{v}\rho_{23}(\vec{v}). \tag{A4}$$

After integrating Eq. (A4) to the whole velocity group, one can obtain the appropriate expressions for the absorption of the probe beam such as Eq. (2).

APPENDIX B: RATE EQUATION MODEL FOR A THREE-LEVEL, Λ-TYPE SYSTEM

Here, we describe the complete rate equations which are exactly same as the density-matrix model except the coherences. The rate equations in the theoretical model in Fig. 8(a) can be written as

$$\dot{N}_1 = R_1(N_2 - N_1) + \Gamma_1 N_2 - \gamma N_1 + \lambda_1,$$

$$\dot{N}_2 = R_1(N_1 - N_2) + R_2(N_3 - N_2) - \Gamma N_2 + \lambda_2,$$

$$\dot{N}_3 = R_2(N_2 - N_3) + \Gamma_2 N_2 - \gamma N_3 + \lambda_3, \tag{B1}$$

where R_i is the optical pumping rate and can be written as

$$R_i = \frac{\Omega_i^2}{\Gamma}\frac{1}{1 + (2\Delta_i/\Gamma)^2}, \quad (i = 1,2). \tag{B2}$$

After simple algebra assuming no thermal populations in the excited state $N_{20}=0$ and the unity total populations $N_t=N_1+N_2+N_3+N_L=1$, the steady-state expression of the population difference ΔN_{32}^{ss} can be obtained to be

$$\Delta N_{32}^{ss} = N_3^{ss} - N_2^{ss} = N_{31}^0\frac{\gamma(3R_1 + \Gamma)}{2\gamma\Gamma + R_2(3\gamma + \Gamma + \Gamma_1 - \Gamma_2)}\frac{1}{1 + s_{\mathrm{eff}}^{\mathrm{RE}}} + (1 - N_L^{ss})\frac{[\gamma\Gamma + R_1(\Gamma - \Gamma_1 + \Gamma_2)]}{2\gamma\Gamma + R_2(3\gamma + \Gamma + \Gamma_1 - \Gamma_2)}\frac{1}{1 + s_{\mathrm{eff}}^{\mathrm{RE}}}, \tag{B3}$$

where $\Gamma=\Gamma_1+\Gamma_2+\Gamma_L$, Γ_L is the decay rate of the excited state into the uncoupled states, and N_L^{ss} is the population in the uncoupled state indicating the leakage. The saturation parameter from the rate equation model, $s_{\mathrm{eff}}^{\mathrm{RE}}$, is defined by

$$s_{\text{eff}}^{\text{RE}} = \frac{\Omega_1^2}{\Gamma^2} \frac{\frac{\Gamma^2}{\Omega_2^2}(3\gamma + \Gamma - \Gamma_1 + \Gamma_2) + 6\Gamma}{(3\gamma + \Gamma + \Gamma_1 - \Gamma_2) + 2\gamma\frac{\Gamma^2}{\Omega_2^2}}$$

$$\approx \frac{\Omega_1^2}{\Gamma}\left[\frac{3}{2}\frac{1}{\Gamma} + \frac{1}{2\gamma}\left(1 - \frac{\Gamma_1 - \Gamma_2}{\Gamma}\right)\right], \qquad \text{(B4)}$$

where we assume that the square of the probe Rabi frequency is much smaller than other frequency scales ($\Omega_2^2 \ll \Gamma^2$, $\gamma\Gamma^2/\Gamma_i$, $\gamma\Gamma$). The form of $s_{\text{eff}}^{\text{RE}}$ is similar to that of $s_{\text{eff}}^{\text{DM}}$ and the slight difference between them can be attributed to the usage of the different model. Figure 10 shows the $s_{\text{eff}}^{\text{DM}}$ and $s_{\text{eff}}^{\text{RE}}$ as a function of the Rabi frequency of the coupled pump beam.

The effective saturation intensity for the experimental value of γ is found at the low pump Rabi frequency $\Omega_1 = 0.054\Gamma$ ($I_{\text{sat}}^{\text{eff}} = 1.9$ mW/cm^2) from the rate equation model and $\Omega_1 = 0.043\Gamma$ ($I_{\text{sat}}^{\text{eff}} = 1.2$ mW/cm^2) from the density-matrix model which are 1 order of magnitude smaller than that deduced by the two-level system (16 mW/cm^2). For the given parameters in Table II, the $s_{\text{eff}}^{\text{RE}}$ is calculated to be 86 which is comparable to $s_{\text{eff}}^{\text{DM}} = 137$ from the density-matrix model.

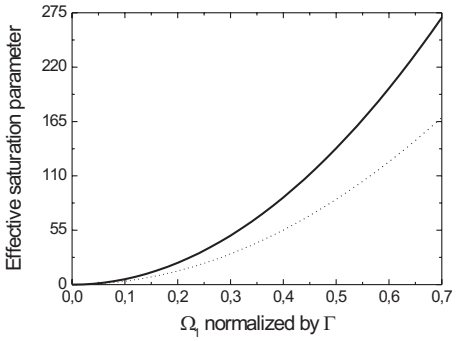

FIG. 10. The effective saturation parameter deduced by the density-matrix model (solid line) and the rate equation model (dotted line) (see also Fig. 9).

[1] W. Demtröder, *Laser Spectroscopy. Basic Concepts and Instrumentation*, 3rd ed. (Springer-Verlag, Berlin, 2002).

[2] C. Wieman and T. W. Hänsch, Phys. Rev. Lett. **36**, 1170 (1976).

[3] B. Klöter, C. Weber, D. Haubrich, D. Meschede, and H. Metcalf, Phys. Rev. A **77**, 033402 (2008).

[4] J. I. Kim, D. Haubrich, and D. Meschede, Opt. Express **17**, 21216 (2009).

[5] D. Meschede and H. Metcalf, J. Phys. D **36**, R17 (2003).

[6] U. Rasbach, J. Wang, R. dela Torre, V. Leung, B. Klöter, D. Meschede, T. Varzhapetyan, and D. Sarkisyan, Phys. Rev. A **70**, 033810 (2004).

[7] M. S. Feld, M. M. Burns, T. U. Kühl, P. G. Pappas, and D. E. Murnick, Opt. Lett. **5**, 79 (1980).

[8] P. G. Pappas, M. M. Burns, D. D. Hinshelwood, M. S. Feld, and D. E. Murnick, Phys. Rev. A **21**, 1955 (1980).

[9] O. Schmidt, K.-M. Knaak, R. Wynands, and D. Meschede, Appl. Phys. B: Lasers Opt. **59**, 167 (1994).

[10] B. E. Sherlock and I. G. Hughes, Am. J. Phys. **77**, 111 (2009).

[11] K.-J. Boller, A. Imamoğlu, and S. E. Harris, Phys. Rev. Lett. **66**, 2593 (1991).

[12] E. Arimondo, in *Progress in Optics*, edited by E. Wolf (Elsevier, Amsterdam, 1996), Vol. 35, p. 257.

[13] P. R. Berman, P. F. Liao, and J. E. Bjorkholm, Phys. Rev. A **20**, 2389 (1979).

[14] J. I. Kim, C. Y. Park, J. Y. Yeom, E. B. Kim, and T. H. Yoon, Opt. Lett. **28**, 245 (2003).

[15] C. Y. Park and T. H. Yoon, Jpn. J. Appl. Phys. **42**, L754 (2003).

[16] B. Smeets, R. C. M. Bosch, P. van der Straten, E. te Sligte, R. E. Scholten, H. C. W. Beijerinck, and K. A. H. van Leeuwen, Appl. Phys. B: Lasers Opt. **76**, 815 (2003).

[17] O. M. Maragò, B. Fazio, P. G. Gucciardi, and E. Arimondo, Appl. Phys. B: Lasers Opt. **77**, 809 (2003).

[18] P. R. Berman, in *Advances in Atomic and Molecular Physics*, edited by D. R. Bates and B. Bederson (Academic, New York, 1977), Vol. 13, p. 57.